Desalination and Water Treatment
www.deswater.com

doi: 10.1080/19443994.2015.1025851

57 (2016) 8826–8838
April

Taylor & Francis
Taylor & Francis Group

Synthesized multi-walled carbon nanotubes as a potential adsorbent for the removal of methylene blue dye: kinetics, isotherms, and thermodynamics

Veyis Selen[a,*], Ömer Güler[b], Dursun Özer[a], Ertan Evin[b]

[a]*Department of Chemical Engineering, Firat University, 23279 Elazig, Turkey, Tel. +90 424 237 0000, ext. 5522; Fax: +90 424 241 5526; email: vselen@firat.edu.tr (V. Selen), Tel. + 90 424 237 0000, ext. 5518; Fax: +90 424 241 5526; email: dozer@firat.edu.tr (D. Özer)*

[b]*Department of Metallurgical and Materials Engineering, Firat University, 23279 Elazig, Turkey, Tel. +90 424 237 0000, ext. 6381; Fax: +90 424 241 5526; email: oguler@firat.edu.tr (Ö. Güler), Tel. +90 424 237 0000, ext. 6372; Fax: +90 424 241 5526; email: eevin@firat.edu.tr (E. Evin)*

Received 4 August 2014; Accepted 27 February 2015

ABSTRACT

Multi-walled carbon nanotubes (MWCNTs) are a highly effective adsorbent of methylene blue (MB), and they can be used to remove MB from aqueous solutions. In this study, we used MWCNTs that were synthesized by chemical vapor deposition method. The physico-chemical properties of MWCNTs were characterized by Brunauer-Emmett-Teller (BET) surface area, surface functional group analysis by fourier transform infrared (FTIR) analysis, zero point charge (pH_{zpc}), X-ray diffraction (XRD), and transmission electron microscopy (TEM). The factors that affected the adsorption properties of MB onto MWCNTs were investigated, including initial pH, contact time, dosage, initial concentration, and temperature. The equilibrium adsorption data were analyzed using two common adsorption models, i.e. the Langmuir and Freundlich models. The results indicated that the Langmuir isotherm fits the experimental results well. The maximum adsorption capacity obtained from the equation of the Langmuir isotherm at 323 K was 95.30 mg/g, indicating that the MWCNTs adsorbed MB effectively. The kinetic study illustrated that the adsorption of MB onto MWCNTs fits the pseudo-second-order kinetic model. The thermodynamic parameters indicated that the adsorption of MB onto MWCNTs was a spontaneous, endothermic process.

Keywords: Multi-walled carbon nanotubes (MWCNTs); Methylene blue (MB); Adsorption; Kinetics; Thermodynamic parameters

1. Introduction

The effluents from industries that use dyes, such as the printing, food, textiles, ink, cosmetics, plastic, and related industries, are the one of main causes of environmental pollution [1]. These dye molecules are toxic to people and micro-organisms. Many thousands of different dyes have been used in industry for many years [2]. The most well known of these harmful dyes is methylene blue (MB), which is a cationic dye that is the most commonly used substance for dying cotton, wood, and silk [3]. MB is not considered to be a very toxic dye, but it can cause people to experience some harmful effects, such as vomiting, increased heart rate, diarrhea, shock, cyanosis, jaundice, quadriplegia, and tissue

*Corresponding author.

necrosis [4]. Therefore, many different ways are used to remove MB and other harmful dyes from industrial wastes. Many physical, chemical, and biological processes have been investigated for this purpose, including adsorption [5,6], biosorption [7], photodecomposition [8], and ultrafiltration [9].

Among these methods, adsorption is the most widely used because of the ease of operation and it's comparatively low cost. In addition, adsorption has been proven to be more effective for the treatment of dyes [10]. The adsorbents that are used for adsorption must be low cost, easily available, renewable, and low toxicity. Various adsorbents have been studied for the adsorption of MB from aqueous solutions, including bamboo-activated carbon [11], jute fiber carbon [12], cedar sawdust and crushed brick [13], unburned carbon [14], bentonite [15], modified expanded graphite power [16], and carbon nanotubes [17], and some of them have been found to adsorb MB effectively.

With the development of nanotechnology in recent years, various nanomaterials have been used extensively in adsorption, including carbon nanotubes (CNTs), graphene, and graphene oxide. In comparison with classical adsorbents, such as activated carbon and clay, CNTs are a more attractive alternative for the removal of dye contaminants from aqueous effluents. This is because their favorable physicochemical stability, high selectivity, large specific surface area, small size, and hollow and layered structures provide much higher sorption capacity than traditional adsorbents [18,19].

The multi-walled carbon nanotubes (MWCNTs) production is more and more easier via many studies for years. The effective and easy production methods cause to decrease MWCNTs price. MWCNTs are a good candidate because of both price decrease and excellent properties of MWCNTs for the adsorption process. In this study, cheap MWCNTs products were synthesized by simple chemical vapor deposition (CVD) method. In addition, our MWCNTs were behaved as a good adsorbent for MB adsorption although no surface modification was done to produced nanotubes.

The primary aim of this study was to evaluate the adsorption potential of MWCNTs for removing MB from aqueous solutions. The influences of the various experimental parameters were investigated, including initial pH, contact time, the dosage of MWCNTs, the initial concentration of the MB, and temperature. The experimental data were analyzed using Langmuir and Freundlich isotherms, and some thermodynamic and kinetic parameters were calculated for the adsorption process. The kinetic data were analyzed in order to determine the adsorption mechanisms, and different models, i.e. a pseudo-first-order kinetic model, a pseudo-second-order kinetic model, and an intraparticle diffusion adsorption model, were used to fit the experimental data. Moreover, the obtained MWCNTs were characterized by BET surface area, surface functional group analysis by FTIR analysis, zero point charge (pH_{zpc}), XRD, and TEM.

2. Experimental

2.1. Preparation of MWCNTs

MWCNTs were grown onto p-doped Si (1 0 0) substrates that were rinsed consecutively in acetone and ethanol in an ultrasonic bath prior to their being placed in the vacuum chamber. Nano-Fe particles were distributed onto the Si wafers to act as a catalyst. Distributed Fe particles were obtained by a ball milling process. The substrates were inserted into the center of a quartz tube reactor housed in a furnace. The tube was evacuated at a base pressure of 10^{-3} torr by a rotary pump for purging. The furnace was heated to 923 K under an Ar gas atmosphere (1 L/min) at 2 torr and after the heating process, the C_2H_2 gas flow had the same pressure for 40 min at fixed 923 K. Then, the furnace was made cool while maintaining the Ar atmosphere. In order to remove the amorphous carbon structures obtained inside the powder, the powder was kept in a mixture of nitric acid and hydrochloric acid for 3 h. Then, the powders were rinsed with distilled water and dried in an oven at 423 K for 10 h. The obtained MWCNTs were characterized by BET surface area (Micromeritics ASAP 2020), XRD diffraction (Bruker Advance D8, CuK_α), TEM (Jeol Jem 2100F), and FTIR (ATI Unicam Mattson 1000 Fourier Transform Infrared Spectrophotometer).

2.2. Preparation of methylene blue

All of the primary chemicals that were used were of analytical grade. MB (Table 1, Fig. 1), caustic soda (NaOH), nitric acid (HNO_3), and hydrochloric acid (HCl) were purchased from Merck Chemicals (Darmstadt, Germany) and used without any further purification. A stock solution of MB (1,000 mg/L) was prepared by dissolving the required amount of MB in

Table 1
Characterization of methylene blue

Generic name	CI Basic Blue 9
Molecular formula	$C_{16}H_{18}N_3SCl$
λ_{max} (nm)	660
Molecule weight (g/mol)	319.85

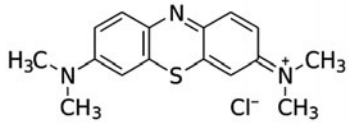

Fig. 1. Chemical structure of methylene blue.

a given volume of distilled water. Working solutions of MB dye solutions were prepared by diluting the stock MB solution with distilled water. Solutions of caustic soda (0.1 M) and hydrochloric acid (0.1 M) were used to adjust the pH of the working solutions to the required values.

2.3. Experimental methods

All experiments were conducted in a closed, 1,000 mL, glass, round-bottom flask. The flask, which contained the MWCNTs and 600 mL of the MB solution, was placed in a thermostatic water bath and mixed at 600 rpm for 60 min. The experiments to determine the effect of contact time were performed at 293 K for contact periods ranging from 0 to 60 min using 0.25 g/L of MWCNTs and an initial MB concentration of 40 mg/L at pH 5.5–11.0. In the experiments to identify the effect of MB concentration (MWCNTs = 0.25 g/L and T = 293 K), the dye concentrations were 20 and 60 mg/L. In the experiments to determine the effect of the dosage of the MWCNTs (MB concentration = 40 mg/L and T = 293 K), the dosages were 0.15 and 0.5 g/L. In the experiments to establish the effect of temperature (MWCNTs = 0.25 g/L and MB concentration = 40 mg/L), two different temperatures were evaluated, i.e. 293 and 323 K. To obtain equilibrium data for the isotherm studies, 600 mL volumes of the MB solutions with different initial concentrations, ranging from 20 to 70 mg/L, were in contact with 0.15 g of the MWCNTs in a closed, 1,000 mL, glass, round-bottom flask at constant temperature. These experiments were conducted at a constant initial pH value of 10.0 for a contact period of 60 min. At the end of equilibrium period, suspensions were centrifuged at 18,000 rpm for 3 min, and the MB concentration in the supernatant was determined with a UV–vis spectrophotometer (Chebios Optimum-One UVVIS) at 660 nm. The amount of MB adsorbed (mg/g) and the removal efficiency (%) were computed as follows:

$$q_t\ (\mathrm{mg/g}) = \frac{(C_0 - C_t) \times V}{M} \quad (1)$$

$$\text{Removal efficiency}\ (\%) = \frac{(C_0 - C_t)}{C_0} \times 100 \quad (2)$$

where C_0 is the initial concentration of MB (mg/L), C_t is the concentration at any time, t (mg/L), V is the volume of the solution (L), and M is the mass of the adsorbent (g).

In order to understand the adsorption mechanism, it is necessary to determine the zero point charge (pH_{zpc}) of the MWCNTs. The pH at the zero point charge of the MWCNTs was measured using the pH drift method [20–22]. The pH of a solution of 0.01 M NaCl was adjusted between 2 and 12 by adding either HCl or NaOH. The MWCNTs (0.15 g) were added to 50 ml of the solution. Nitrogen was bubbled through the solution at 298 K to remove dissolved carbon dioxide (CO_2) until the initial pH stabilized. The final pH, reached after 24 h in orbital shaker, was measured and plotted against the initial pH. The plot was used to determine the points at which initial pH and final pH values were equal (Fig. 2). This point was taken as the pH_{zpc} of the MWCNTs.

3. Results and discussion

3.1. Characterizations of MWCNTs

In this study, the MWCNTs that were used as the absorbent material were synthesised by the method of chemical vapor deposition. Fig. 3 illustrates the XRD pattern of the product obtained at the end of the process. XRD analysis of the product was performed by Diffracplus Evaluation Software, and the International Centre for Diffraction Data tag number

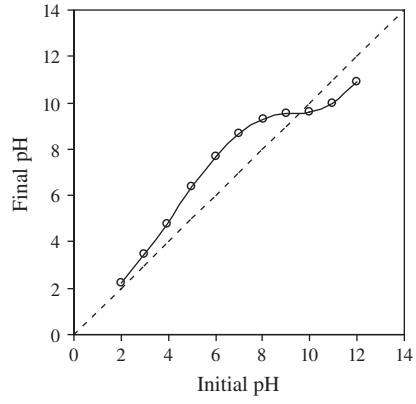

Fig. 2. Plot of final pH against initial pH for the pH drift method to obtain the pH_{zpc}.

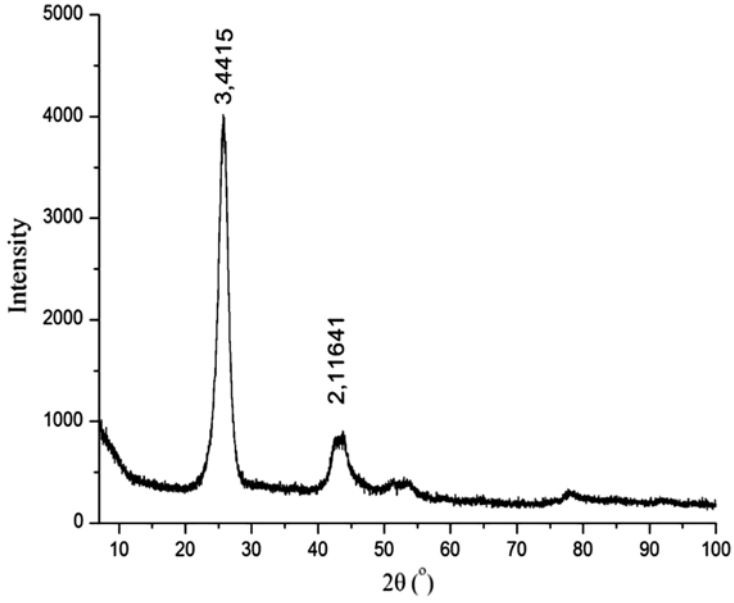

Fig. 3. XRD pattern of synthesized carbon nanotubes by the CVD method.

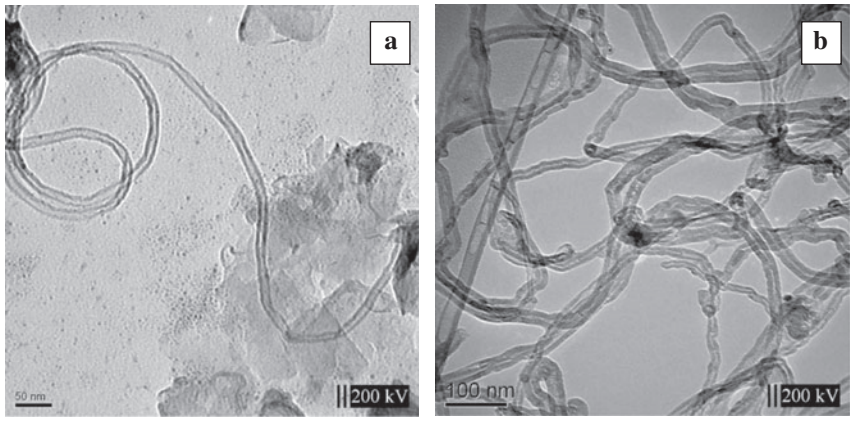

Fig. 4. TEM images of carbon nanotubes synthesized by the CVD method: (a) before acid treatment and (b) after acid treatment.

was 00-058-1638. According to this tag number, these peaks were due to the carbon nanotubes in the software. The strong peak at approximately 26˚ was the MWCNT peak. This peak is the (0 0 2) peak, and it also was observed in the hexagonal graphite structure. The peak at approximately 42˚ was the (1 0 0) peak.

Fig. 4(a) and (b) illustrate the TEM images that were taken from the product that was obtained. The image in Fig. 4(a) is the image of the MWCNTs that were synthesized before the acid treatment. The image in Fig. 4(b) is the TEM image of the specimen after the acid process was used to eliminate amorphous carbon structures. As both images show, dense MWCNTs were present in the structure, and, according to their TEM images, the diameters of these tubes averaged 20–30 nm, and their lengths were about 1–2 μm. Some of the catalyst particles that were used during the synthesis process were on the ends of the MWCNTs. Also, the MWCNTs were in the form of bundles. Fig. 4(a) illustrates the densely transparent sheets. These sheets were amorphous carbon structures that could be not converted to nanotubes during the decomposition of the C_2H_2 gas. Also, there were dense, black particles in the bundle of MWCNTs. These particles are the nano-iron particles that

function as a catalyst. MWCNTs nucleate and grow on these particles.

Fig. 4(b) shows that there is essentially no amorphous carbon in the structure. This situation shows that keeping the powder in the acid mixture successfully eliminated amorphous carbon. Furthermore, it was apparent that the quantity of nano-dimensional iron particles was reduced significantly, but it was not possible to say that none of them were present. The acid mixture had no effect, especially on the particles that were wrapped with the nanotube walls and on which MWCNTs grew. In other words, the MWCNTs formed a protective medium for these particles.

The single-point BET surface area of the MWCNTs was determined by the nitrogen adsorption method to be 118.9 m^2/g, and the average diameter of the pores was determined to be 21.74 Å using a Micromeritics ASAP 2020 apparatus. The pore volume was estimated as 0.0646 cm^3/g.

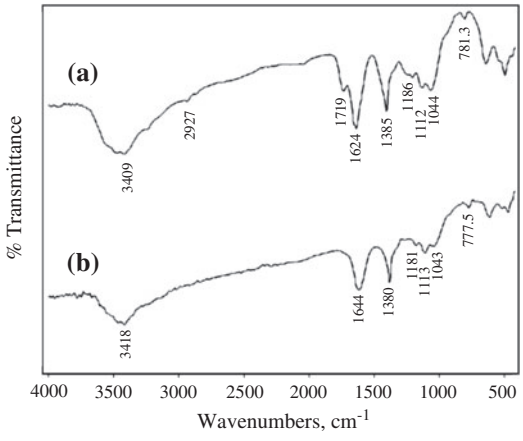

Fig. 5. FTIR spectra of MWCNTs before (a) and after (b) adsorption of MB at pH 10.0.

Fourier transform infrared (FTIR) spectroscopy was used to identify the functional groups on the surface of MWCNTs. FTIR spectral peaks were collected between 400 and 4,000 cm^{-1} by averaging 16 scans. Fig. 5 shows the FTIR spectra of the MWCNTs before and after adsorption of MB at pH 10.0. The major peaks are presented in Table 2. The peaks' shifts indicated that especially the bonded –OH groups, phenols and alcohols; C–H stretching, nonionic carboxyl groups; C=O stretching, carboxyl groups; C=C stretching, aromatic ring; C–H bending, methyl and phenol alcohols; C–O stretching, ether groups; and –C–C– group played a major role in MB adsorption on MWCNTs. Researchers reported similar results in the literature [23–26].

3.2. Effect of contact time and initial pH

The influence of pH on the removal of MB by adsorption on MWCNTs was studied by varying the pH values from 5.5 to 11.0 and using a contact time of 60 min at each pH value at 293 K. The uptake of MB from solution by the MWCNTs increased with contact time, with equilibrium being attained at 60 min. The pH had a significant effect on the adsorption of MB by the MWCNTs, as evidenced by the drastic changes in the adsorption percentage as a function of the pH of the solutions. The pH of the system had a profound influence on the uptake of adsorbate molecules, presumably due to its influence on the surface properties of the adsorbent and on the ionization/dissociation of the adsorbate's molecules [18]. Fig. 6 shows the results. The amount of MB that was adsorbed was found to increase linearly with the increase in pH from 5.5 to 10.0, and the adsorption levels of MB decreased sharply as the pH increased from 10.0 to 11.0. The optimum pH value for the maximum adsorption of MB was determined to be 10.0, at which

Table 2
The comparison of FTIR spectral characteristics of MWCNTs before and after MB adsorption

IR peak	Frequency (cm^{-1})		Assignment
	Before adsorption	After adsorption	
1	3,409	3,418	Bonded –OH groups
2	2,927	–	C–H stretching
3	1,719	–	C=O stretching
4	1,624	1,644	C=C stretching
5	1,385	1,380	C–H bending
6	1,186	1,181	C–O stretching
7	1,112	1,113	C–O stretching
8	1,044	1,043	–C–C– group
9	781.3	777.5	–C–C– group

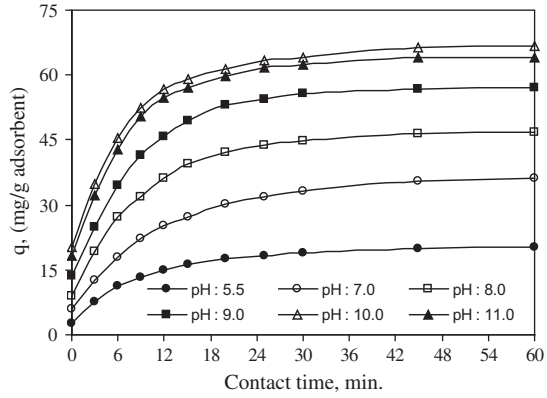

Fig. 6. Effect of contact time and initial pH on the adsorption of MB by MWCNTs (conditions: 0.15 g MWCNTs, 600 mL of the 40 mg MB/L solution, contact temperature: 293 K).

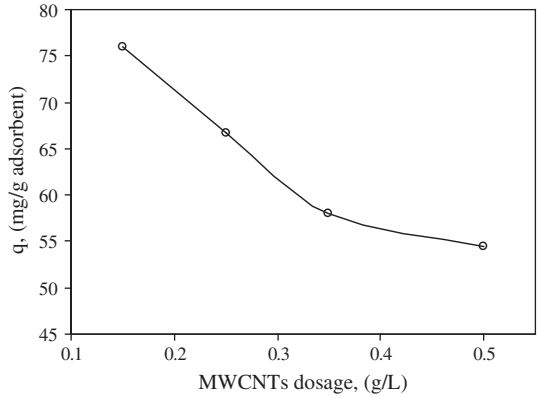

Fig. 7. Effect of adsorbent dosage on the adsorption of MB by MWCNTs (conditions: $pH_{initial}$: 10.0; 600 mL of 40 mg/L MB solution; contact temperature: 293 K).

the amount of MB adsorbed and the percentage of the MB removed were determined to be 66.7 mg/g and 41.7%, respectively. The reason of this situation can be explained by the zero point charge (pH_{zpc}) of the MWCNTs (pH_{zpc} = 9.65). At lower pH values, the excess hydrogen ions (H^+) competed with the dye cations for the active sites on the surface of the adsorbent, and the decrease in the number of available sites for MB molecules resulted in a lower adsorptive capacity [1]. MWCNTs are negatively charged in solution due to the presence of oxygen-containing functional groups. When the solution pH is greater than pH_{zpc}, the surface of MWCNTs had more negative charges, which enhanced the electrostatic interaction between the positively charged dye and the composite adsorbent. The enhanced electrostatic attractive forces resulted in increased uptake of dye molecules from the water [27].

3.3. *Effects of the dosage of the adsorbent and initial concentration of the dye*

The effect of the adsorbent's dosage on the capacity of the MWCNTs to remove MB from the solution was investigated with different dosages of the adsorbent in the range of 0.15–0.50 g/L at 293 K, initial pH of 10.0, and an initial dye concentration 40 mg/L (Fig. 7). The amount of MB adsorbed decreased from 76.0 mg/g for an absorbent mass of 0.15 g/L–54.5 mg/g for an absorbent mass of 0.50 g/L, whereas the percentage of color removal increased from 28.5 to 68.1 % when the adsorbent mass was increased from 0.15 to 0.50 g/L. This is due to the increase in surface area resulting from the increase in adsorbent mass, thus increasing the number of active adsorption sites [28]. The amount of dye adsorbed per unit mass of adsorbent decreased with increasing adsorbent mass due to the reduction in effective surface area. This may be also attributed to overlapping or aggregation of adsorption sites, resulting in a decrease in total surface area of adsorbent available to the dye and an increase in diffusion path length [5,29].

The effect of the initial concentration of the dye on its adsorption onto MWCNTs was investigated for the range of 20–60 mg/L, while the temperature, initial pH, and adsorbent dosage were kept at 293 K, 10.0, and 0.25 g/L, respectively (Fig. 8). The initial concentration provides an important driving force to overcome all mass transfer resistances of the dye between the aqueous and solid phases. Hence, a higher initial concentration of dye will enhance the adsorption process [30].

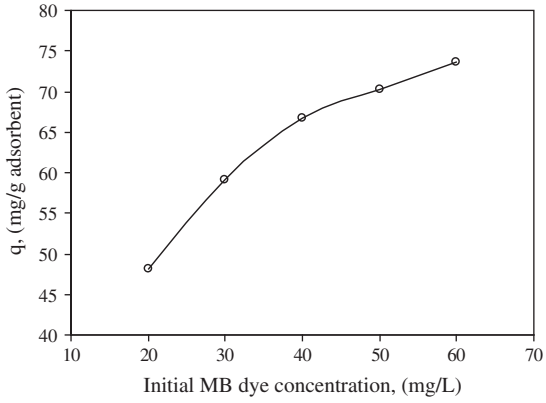

Fig. 8. Effect of initial dye concentration on the adsorption of MB by MWCNTs (conditions: $pH_{initial}$: 10.0; 0.15 g MWCNTs; 600 mL of the MB solution; contact temperature: 293 K).

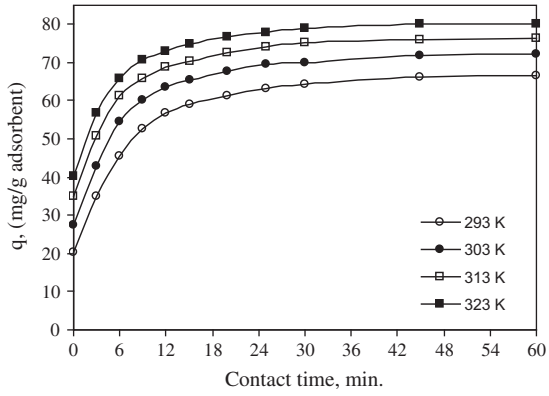

Fig. 9. Effect of temperature on the adsorption of MB by MWCNTs (conditions: $pH_{initial}$: 10.0; 0.15 g MWCNTs; 600 mL of 40 mg/L MB solution).

3.4. Effect of temperature

Time-dependent adsorption experiments were conducted at 293, 303, 313, and 323 K to investigate the effect of temperature, and Fig. 9 shows the results of these experiments. A comparison of the adsorption values at different temperatures shows that the adsorption capacity increased as the temperature increased, with an increase in temperature from 293 to 323 K increases the amount of MB adsorbed by the MWCNTs from 66.72 to 80.16 mg/g. This may be a result of the increase in the mobility of the dye molecules with increasing temperature. An increasing number of molecules may also acquire sufficient energy to undergo an interaction with active sites at the surface [31]. Furthermore, the major effect of temperature was influenced by the diffusion rate of the adsorbate molecules and the internal pores of the adsorbent particles. An increase in the temperature decreased the viscosity of the solution, thereby increasing the rate of diffusion of the adsorbate molecules across the external boundary layer and within the internal pores of the adsorbent particles [32]. The increases of the equilibrium uptake with increasing temperature indicated that the MB adsorption process was endothermic.

3.5. Adsorption kinetics

Adsorption kinetic studies are very important in the treatment of wastewater because they can provide valuable information on the mechanism of the adsorption process [33]. In order to understand the detailed characteristics of the adsorption processes of MB on MWCNTs, kinetic analyses were conducted using a pseudo-first-order kinetic model and a pseudo-second-order kinetic model. The kinetic parameters for the adsorption process were studied at the MB concentration of 40 mg/L for temperatures ranging from 293 to 323 K by monitoring the amount of MB adsorbed by MWCNTs.

3.5.1. Pseudo-first-order kinetic model

The pseudo-first-order equation, proposed by Lagergren [34], is the most popular kinetics equation, and it was used only for the rapid initial phase. The pseudo-first-order equation is given by:

$$\log(q_{eq} - q_t) = \log q_{eq} - \frac{k_1 t}{2.303} \quad (3)$$

Table 3
Pseudo-first- and pseudo-second-order kinetic models' constants at different temperatures for the adsorption of MB onto MWCNTs (conditions: 600 mL of 40 mg/L MB solution; 0.15 g MWCNTs; $pH_{initial}$:10.0)

Pseudo-first-order kinetic model				
Temperature (K)	q_{eq} (mg/g)	$q_{eq,cal}$ (mg/g)	k_1*10^3 (min^{-1})	R^2
293	66.72	37.52	97.19	0.980
303	72.32	34.89	99.49	0.974
313	76.45	32.92	108.9	0.987
323	80.16	30.27	108.7	0.982
Pseudo-second-order kinetic model				
Temperature (K)	q_{eq} (mg/g)	$q_{eq,cal}$ (mg/g)	k_2*10^3 (g/mg min)	R^2
293	66.72	68.97	6.295	0.998
303	72.32	74.07	7.856	0.999
313	76.45	78.13	9.695	0.999
323	80.16	81.30	11.04	0.999

where q_t is the amount of adsorption at any time (mg/g), k_1 is the rate constant of the equation (l/min), q_e is the amount of adsorption equilibrium (mg/g), and t is the time (min).

The rate constant k_1, correlation coefficients, experimental (q_{eq}), and predicted ($q_{eq,cal}$) values of the MB under single concentration were calculated from the linear plot of log ($q_{eq} - q_t$) vs. t (figure not shown) and listed in Table 3.

3.5.2. Pseudo-second-order kinetic model

The pseudo-second-order kinetic model based on the amount of adsorption can be expressed as [17]:

$$\frac{t}{q_t} = \frac{1}{k_2 q_{eq}^2} + \frac{t}{q_{eq}} \tag{4}$$

where q_t is the amount of adsorption at any time (mg/g); k_2 is the rate constant of the pseudo-second-order model (g/mg min); q_{eq} is the amount of adsorption equilibrium (mg/g), and t is the time (min). The plot of t/q_t vs. t should give a straight line if the pseudo-second-order kinetic is applicable to the adsorption of MB onto MWCNTs (figure not shown). The values of $q_{eq,cal}$ and k_2 can be determined from the slope and intercept of the plot, respectively. The rate constant k_2, correlation coefficients, and predicted ($q_{eq,cal}$) values are presented in Table 3.

The data in Table 3 indicate that the correlation coefficients for the pseudo-first-order kinetic model were low at all of the temperatures that were studied. In contrast, the use of the pseudo-second-order kinetic model provided much better regression coefficients, all of which were greater than 0.99. Also, it was observed that the adsorption capacity values ($q_{eq,cal}$) calculated by the pseudo-first-order kinetic model deviated considerably from the experimental values (q_{eq}). However, in the pseudo-second-order kinetic model, the calculated adsorption capacity values ($q_{e,cal}$) were very close to the experimental values at all of the temperatures that were studied. As a result, it can be concluded that the adsorption of MB by the MWCNTs takes place according to the pseudo-second-order kinetic model. Similar results have been reported by many studies for MB adsorption by different materials [17,33,35].

3.5.3. The intraparticle diffusion model

Since neither the pseudo-first-order model nor the pseudo-second-order model can identify the diffusion mechanism, an intraparticle mass transfer diffusion model proposed by Weber and Morris was used for that purpose [18]:

$$q_t = k_{id} t^{1/2} + C \tag{5}$$

where C is the intercept and k_{id} is the intraparticle diffusion rate constant (mg/g min$^{1/2}$), which can be evaluated from the slope of the linear plot of q_t vs. $t^{1/2}$ (Fig. 10). Fig. 10 shows the pore diffusion plot of MB adsorption on MWCNTs as the temperature varies from 293 to 323 K. Fig. 8 shows that the plots are not linear over the entire time range, implying that more than one process affected the adsorption. If intraparticle diffusion occurs, then q_t vs. $t^{1/2}$ will be linear, and, if the plot passes through the origin, then the rate-limiting process is only due to intraparticle diffusion [32]. The multiple natures of these plots could be explained by boundary layer diffusion, which gave the first portion, and intraparticle diffusion, which produced two linear portions. If the intraparticle diffusion was the only rate-controlling step, the plot would pass through the origin; if not, boundary layer diffusion controlled the adsorption to some degree. It could be deduced that there were three processes that controlled the rate of adsorption of the dye molecules, but only one of the processes was rate limiting in any particular time range [36].

The activation energy (E_a) for the adsorption of MB can be calculated by the linear Arrhenius equation Eq. (6). The pseudo-second-order rate constant is expressed as a function of temperature by the linear-type Arrhenius equation:

$$\ln (k_2) = \ln (A) - \frac{E_a}{RT} \tag{6}$$

where A (time^{-1}) is the frequency factor, E_a (J/mol) is the activation energy of the adsorption reaction, R (8.314 J/mol.K) is the universal gas constant, and T (K) is the temperature of the solution. By plotting ln (k_2) vs. $1/T$, the activation energy can be calculated from the slope (figure not shown). The activation energy was determined to be 14.96 kJ/mol for the adsorption of MB by MWCNTs.

3.6. Adsorption isotherm

Adsorption isotherms are the basic requirements for designing any sorption system [37]. The adsorption capacity is an important factor because it determines how much of an adsorbent is required for quantitative enrichment of adsorbate from a given solution [38]. In

this study, the Langmuir and Freundlich isotherm models were applied to the equilibrium data of the adsorption of MB dye on MWCNTs. Figs. 11 and 12 show the experimental and predicted isotherms for MB adsorption, respectively. The isotherm constants were determined using the nonlinear regression program of Polymath 6.1 software, which uses the Levenberg–Marquardt algorithm to determine the values of the parameters that minimize the sum of the squares of the errors.

The Langmuir model suggested that pollutant removal from the aqueous phase occurred on homogeneous surfaces by monolayer sorption without interactions between sorbed molecules [39]. The Langmuir isotherm model is given by Eq. (7):

$$q_{eq} = \frac{K_a q_{max} C_{eq}}{1 + K_a C_{eq}} \tag{7}$$

where q_{eq} (mg/g) and C_{eq} (mg/L) are the amount of adsorbed MB per unit weight of MWCNTs and unadsorbed MB amount in solution at equilibrium, respectively; q_{max} is the maximum amount of the MB per unit weight of adsorbent to form a complete monolayer on the surface bound at high C_{eq} (mg/L), and K_a (L/mg) is a constant related to the energy of adsorption. The term q_{max} denotes a practical limiting adsorption capacity when the surface of the adsorbent is completely covered with adsorbate [40].

The Freundlich isotherm is an empirical equation that can be used to describe heterogeneous systems, and adsorption capacity is related to the concentration of dye at equilibrium [41]. The Freundlich isotherm model is given by Eq. (8):

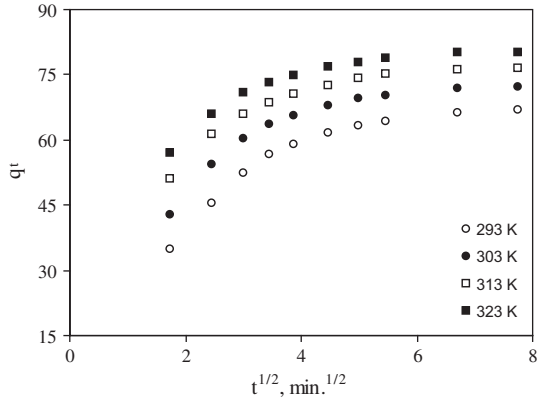

Fig. 10. Plot of q_t against $t^{1/2}$ at different temperatures (conditions: 600 mL of 40 mg/L MB solution; 0.15 g MWCNTs; $pH_{initial}$: 10.0).

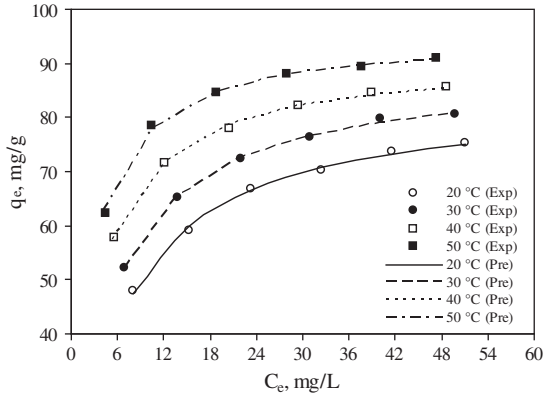

Fig. 11. Comparison of the experimental and predicted Langmuir adsorption isotherms obtained at different fixed temperatures (conditions: 600 mL of MB solution at various concentrations; 0.15 g MWVNTs; $pH_{initial}$: 10.0; contact time: 60 min).

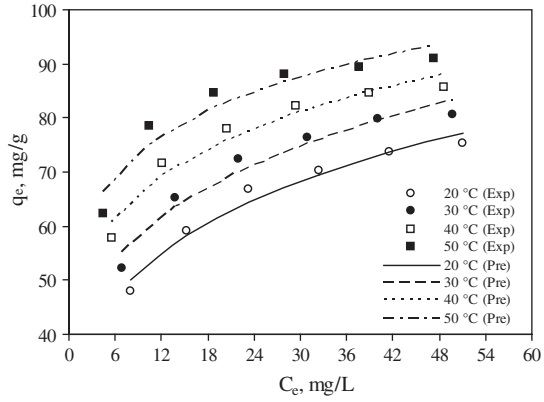

Fig. 12. Comparison of the experimental and predicted Freundlich adsorption isotherms obtained at different fixed temperatures (conditions: 600 mL of MB solution at various concentrations; 0.15 g MWCNTs; $pH_{initial}$: 10.0; contact time: 60 min).

$$q_{eq} = K_f C_{eq}^{1/n} \tag{8}$$

where K_f and $1/n$ are Freundlich constants (capacity and intensity, respectively) that are characteristic of the adsorption system.

Figs. 11 and 12 show the experimental data fitted to the non-linear forms of the Langmuir and Freundlich isotherms for MB adsorption by MWCNTs. The isotherm constants related to the Langmuir and Freundlich models determined from Figs. 10 and 11 are listed in Tables 4 and 5. Linear plots of the Langmuir and Freundlich models were obtained, and the

Table 4
Langmuir model equations and constants at different fixed temperatures for the adsorption of MB onto MWCNTs

	Non-linear model				Linear model			
		Model constants				Model constants		
Temperature (K)	Model equation	q_{max} (mg/g)	K_a (l/mg)	R^2	Model equation	q_{max} (mg/g)	K_a (l/mg)	R^2
293	$q_{eq} = \frac{13.7\ C_{eq}}{1+0.163\ C_{eq}}$	84.2	0.163	0.997	$C_{eq}/q_{eq} = 0.0118\ C_{eq} + 0.0747$	84.7	0.158	0.999
303	$q_{eq} = \frac{18.2\ C_{eq}}{1+0.205\ C_{eq}}$	88.7	0.205	0.999	$C_{eq}/q_{eq} = 0.0112\ C_{eq} + 0.0557$	89.3	0.201	0.999
313	$q_{eq} = \frac{27.8\ C_{eq}}{1+0.304\ C_{eq}}$	91.3	0.304	0.999	$C_{eq}/q_{eq} = 0.0109\ C_{eq} + 0.0367$	91.7	0.297	0.999
323	$q_{eq} = \frac{41.2\ C_{eq}}{1+0.432\ C_{eq}}$	95.3	0.432	0.999	$C_{eq}/q_{eq} = 0.0105\ C_{eq} + 0.0241$	95.2	0.436	1.000

Table 5
Freundlich model equations and constants at different fixed temperatures for the adsorption of MB onto MWCNTs

	Non-linear model				Linear model			
		Model constants				Model constants		
Temperature (K)	Model equation	n	K_f	R^2	Model equation	n	K_f	R^2
293	$q_{eq} = 31.0\ C_{eq}^{1/4.31}$	4.31	31.0	0.973	$\ln q_{eq} = 3.40 + 0.243 \ln C_{eq}$	4.12	30.0	0.974
303	$q_{eq} = 36.8\ C_{eq}^{1/4.80}$	4.80	36.8	0.962	$\ln q_{eq} = 3.57 + 0.220 \ln C_{eq}$	4.55	35.5	0.963
313	$q_{eq} = 45.3\ C_{eq}^{1/5.83}$	5.83	45.3	0.952	$\ln q_{eq} = 3.78 + 0.181 \ln C_{eq}$	5.53	43.9	0.954
323	$q_{eq} = 53.5\ C_{eq}^{1/6.92}$	6.92	53.5	0.918	$\ln q_{eq} = 3.95 + 0.154 \ln C_{eq}$	6.48	52.0	0.919

constants related to the linear form were calculated and listed in Tables 4 and 5, so their values could be compared with those of the non-linear models.

The values of the linear and non-linear regression coefficients in Tables 4 and 5 show that the Langmuir adsorption isotherm model sufficiently fits the experimental data of the adsorption of MB on the MWCNTs. The maximum adsorption capacities q_{max} and the Langmuir constant (K_a) values increased from 84.2 to 95.3 mg/g and 0.163 to 0.432 L/mg, respectively, as the temperature was increased from 293 to 323 K for MB uptake on MWCNTs (Table 4). The values of the Freundlich constant (K_f) increased with increasing temperature and showed easy uptake of MB molecules by the adsorbent. The highest (K_f) value was 53.5 at 323 K (Table 5). All n values were found to be greater than one (>1.0), indicating that the MB molecules were favorably adsorbed by MWCNTs at all of the temperatures that were studied [42]. The values of n in the range of 2–10 represent good adsorption [43]. The maximum adsorption capacity was comparable to the adsorption capacities of some other adsorbents for MB (Table 6). This signified the applicability of MWCNTs as an effective adsorbent for removing cationic dyes from wastewater.

Table 6
Comparison of the monolayer equilibrium adsorptive capacity of various adsorbents for methylene blue basic dye

Adsorbent	q_{max} (mg/g)	References
Carbon nanotubes	64.70	[17]
Magnetic graphene–carbon nanotube composite	65.79	[27]
Graphene oxide	144.9	[44]
Oxalic acid modified rice husk	53.21	[45]
Peanut husk	72.13	[46]
Cylindrical graphene–carbon nanotube hybrid	81.97	[35]
Multi-walled carbon nanotubes (MWCNTs)	95.30	This study

3.7. Determination of thermodynamic parameters

Thermodynamic parameters, such as change in enthalpy (ΔH°), free energy (ΔG°), and entropy (ΔS°), were calculated. The Langmuir isotherm was used to calculate these thermodynamic parameters using the following equations:

$$\ln K_a = \ln K'_a - \frac{\Delta H^\circ}{R}\left(\frac{1}{T}\right) \quad (9)$$

$$\ln\left(\frac{1}{K_a}\right) = \frac{\Delta G^\circ}{R}\left(\frac{1}{T}\right) \quad (10)$$

$$\Delta S^\circ = \frac{(\Delta H^\circ - \Delta G^\circ)}{T} \quad (11)$$

where K_a is the adsorption equilibrium constant obtained from the Langmuir isotherm (L/mol), R is the ideal gas constant (8.314 J/mol K), and T is the absolute temperature. Considering the relationship between ΔG° and K_a, ΔH° and ΔS° were determined from the slope and intercept of van't Hoff plots of ln K_a vs. $1/T$ (figure not shown). The enthalpy change of the process was calculated to be 26.09 kJ/mol. The positive value of ΔH° suggests the endothermic nature of adsorption processes. Physical adsorption and chemisorption can be classified, to a certain extent, by the magnitude of the enthalpy change. It is accepted that bonding strengths of <84 kJ/mol are typically those of physical adsorption-type bonds. Chemisorption bond strengths can range from 84 to 420 kJ/mol [47]. Generally, ΔG° for physical adsorption is less than that for chemisorption. The former is between −20 and 0 kJ/mol, and the latter is between −80 and −400 kJ/mol. In addition, the physical adsorption process normally has an activation energy of 5–40 kJ/mol, while chemisorption has a relatively higher activation energy (40–800 kJ/mol) [48]. Therefore, the values of ΔH° and ΔG° suggest that the adsorption of MB onto MWCNTs occurred by a physical adsorption process. Table 7 shows the calculated values of ΔG° and ΔS° from Eqs. (12) and (13), respectively. The ΔG° values were found to be increasingly negative as temperature increased, indicating that the adsorption of MB onto MWCNTs is a spontaneous process and confirming the affinity of MWCNTs for MB. The positive values of ΔS° confirmed the increased randomness at the solid–solute interference during the adsorption processes, which suggested that molecules of MB dye replaced some water molecules from the solution that were previously adsorbed on the surface of adsorbent [49].

Table 7
Values of thermodynamic parameters for the adsorption of MB by MWCNTs

Temperature (K)	K_a (L/mg)	$-\Delta G^\circ$ (kJ/mol)	ΔS° (kJ/mol K)
293	0.163	26.45	0.179
303	0.205	27.94	0.178
313	0.304	29.89	0.179
323	0.432	31.78	0.179

4. Conclusions

This study showed that MWCNTs particles can effectively remove MB from wastewater. Experiments were performed as a function of initial pH, contact time, dosage of MWCNTs, initial concentration of MB, and temperature. It was observed that the removal amount of MB increased with contact time and reached equilibrium within 60 min. The initial pH and temperature had significant effects on the adsorption capacity of the MWCNTs. The optimum initial pH for the removal of MB was found to be 10.0. The pseudo-second-order kinetic model described the adsorption process with a good fitting. The pseudo-second-order rate constant and activation energy for the process were found to be 0.011 mg/mg min and 14.96 kJ/mol, respectively, at 323 K. The intraparticle diffusion model was used to interpret the adsorption mechanism. The equilibrium data were analyzed using Langmuir and Freundlich isotherm models. The adsorption equilibrium was best described by the Langmuir isotherm model, with maximum monolayer adsorption capacities found to be 84.2, 88.7, 91.3, and 95.3 mg/g at 293, 303, 313, and 323 K, respectively. The thermodynamic parameters of the adsorption process also were evaluated. The positive value of ΔH° (26.09 kJ/mol) indicated that the adsorption process was endothermic. Determining that the ΔG° value was negative verified the spontaneous nature of the adsorption process. The positive value of ΔS° showed that randomness at the solid–solution interface increased during the adsorption process.

References

[1] A. Aluigi, F. Rombaldoni, C. Tonetti, L. Jannoke, Study of methylene blue adsorption on keratin nanofibrous membranes, J. Hazard. Mater. 268 (2014) 156–165.
[2] B.H. Hameed, A.A. Ahmad, Batch adsorption of methylene blue from aqueous solution by garlic peel, an agricultural waste biomass, J. Hazard. Mater. 164 (2009) 870–875.

[3] H. Deng, J.J. Lu, G.X. Li, G.L. Zhang, X.G. Wang, Adsorption of methylene blue on adsorbent materials produced from cotton stalk, Chem. Eng. J. 172 (2011) 326–334.
[4] Y.H. Li, Q.J. Du, T.H. Liu, X.J. Peng, J.J. Wang, J.K. Sun, Y.H. Wang, S.L. Wu, Z.H. Wang, Y.Z. Xia, L.H. Xia, Comparative study of methylene blue dye adsorption onto activated carbon, graphene oxide, and carbon nanotubes, Chem. Eng. Res. Des. 91 (2013) 361–368.
[5] D. Özer, G. Dursun, A. Özer, Methylene blue adsorption from aqueous solution by dehydrated peanut hull, J. Hazard. Mater. 144 (2007) 171–179.
[6] T. Ma, P.R. Chang, P. Zheng, F. Zhao, X. Ma, Fabrication of ultra-light graphene-based gels and their adsorption of methylene blue, Chem. Eng. J. 240 (2014) 595–600.
[7] R. Abdallah, S. Taha, Biosorption of methylene blue from aqueous solution by nonviable *Aspergillus fumigatus*, Chem. Eng. J. 195-196 (2012) 69–76.
[8] W. Ko, S. Jeon, An electrodeless quartz crystal resonator integrated with UV/Vis spectroscopy for the investigation of the photodecomposition of methylene blue, Sens. Actuators, B 193 (2014) 774–777.
[9] Z.N. Shkavro, V.M. Kochkodan, R. Ognyanova, T. Budinova, V.V. Goncharuk, Combined ultrafiltration-adsorption water purification of the cationic violet dye, J. Water Chem. Technol. 32 (2010) 101–106.
[10] A.F. Hassan, A.M. Abdel-Mohsen, M.M.G. Fouda, Comparative study of calcium alginate, activated carbon, and their composite beads on methylene blue adsorption, Carbohydr. Polym. 102 (2014) 192–198.
[11] B.H. Hameed, A.T.M. Din, A.L. Ahmad, Adsorption of methylene blue onto bamboo-based activated carbon: Kinetics and equilibrium studies, J. Hazard. Mater. 141 (2007) 819–825.
[12] S. Senthilkumaar, P.R. Varadarajan, K. Porkodi, C. Subbhuraam, Adsorption of methylene blue onto jute fiber carbon: Kinetics and equilibrium studies, J. Colloid Interface Sci. 284 (2005) 78–82.
[13] O. Hamdaoui, Batch study of liquid-phase adsorption of methylene blue using cedar sawdust and crushed brick, J. Hazard. Mater. 135 (2006) 264–273.
[14] S.B. Wang, L. Li, H.W. Wu, Z.H. Zhu, Unburned carbon as a low-cost adsorbent for treatment of methylene blue-containing wastewater, J. Colloid Interface Sci. 292 (2005) 336–343.
[15] S. Hong, C. Wen, J. He, F.X. Gan, Y.S. Ho, Adsorption thermodynamics of methylene blue onto bentonite, J. Hazard. Mater. 167 (2009) 630–633.
[16] M.F. Zhao, P. Liu, Adsorption of methylene blue from aqueous solutions by modified expanded graphite powder, Desalination 249 (2009) 331–336.
[17] Y.J. Yao, F.F. Xu, M. Chen, Z.X. Xu, Z.W. Zhu, Adsorption behavior of methylene blue on carbon nanotubes, Bioresour. Technol. 101 (2010) 3040–3046.
[18] Y.J. Yao, B. He, F.F. Xu, X.F. Chen, Equilibrium and kinetic studies of methyl orange adsorption on multiwalled carbon nanotubes, Chem. Eng. J. 170 (2011) 82–89.
[19] L.D.T. Prola, F.M. Machado, C.P. Bergmann, F.E. de Souza, C.R. Gally, E.C. Lima, M.A. Adebayo, S.L.P. Dias, T. Calvete, Adsorption of Direct Blue 53 dye from aqueous solutions by multi-walled carbon nanotubes and activated carbon, J. Environ. Manage. 130 (2013) 166–175.
[20] Y.F. Jia, B. Xiao, K.M. Thomas, Adsorption of metal ions on nitrogen surface functional groups in activated carbons, Langmuir 18 (2002) 470–478.
[21] M. Danish, R. Hashim, M.N.M. Ibrahim, O. Sulaiman, Characterization of physically activated *acacia mangium* wood-based carbon for the removal of methyl orange dye, Bioresources 8 (2013) 4323–4339.
[22] M.V. Lopez-Ramon, F. Stoeckli, C. Moreno-Castilla, F. Carrasco-Marin, On the characterization of acidic and basic surface sites on carbons by various techniques, Carbon 37 (1999) 1215–1221.
[23] Ş. Taşar, F. Kaya, A. Özer, Biosorption of lead(II) ions from aqueous solution by peanut shells: Equilibrium, thermodynamic and kinetic studies, J. Environ. Chem. Eng. 2 (2014) 1018–1026.
[24] G. Asgari, B. Ramavandi, S. Sahebi, Removal of a cationic dye from wastewater during purification by *Phoenix dactylifera*, Desalin. Water Treat. 52 (2014) 7354–7365.
[25] K. Huang, Y. Xiu, H. Zhu, Removal of heavy metal ions from aqueous solution by chemically modified mangosteen pericarp, Desalin. Water Treat. 52 (2014) 7108–7116.
[26] S. Sadaf, H.N. Bhatti, S. Ali, K.U. Rehman, Removal of Indosol Turquoise FBL dye from aqueous solution by bagasse, a low cost agricultural waste: Batch and column study, Desalin. Water Treat. 52 (2014) 184–198.
[27] P.F. Wang, M.H. Cao, C. Wang, Y.H. Ao, J. Hou, J. Qian, Kinetics and thermodynamics of adsorption of methylene blue by a magnetic graphene-carbon nanotube composite, Appl. Surf. Sci. 290 (2014) 116–124.
[28] F. Çiçek, D. Özer, A. Özer, A. Özer, Low cost removal of reactive dyes using wheat bran, J. Hazard. Mater. 146 (2007) 408–416.
[29] A.S. Franca, L.S. Oliveira, M.E. Ferreira, Kinetics and equilibrium studies of methylene blue adsorption by spent coffee grounds, Desalination 249 (2009) 267–272.
[30] Z. Aksu, S. Tezer, Equilibrium and kinetic modelling of biosorption of Remazol Black B by *Rhizopus arrhizus* in a batch system: Effect of temperature, Process Biochem. 36 (2000) 431–439.
[31] M. Alkan, S. Çelikçapa, O. Demirbaş, M. Doğan, Removal of reactive blue 221 and acid blue 62 anionic dyes from aqueous solutions by sepiolite, Dyes Pigm. 65 (2005) 251–259.
[32] N. Nasuha, B.H. Hameed, A.T.M. Din, Rejected tea as a potential low-cost adsorbent for the removal of methylene blue, J. Hazard. Mater. 175 (2010) 126–132.
[33] Z.H. Chen, J.W. Fu, M.H. Wang, X.Z. Wang, J.N. Zhang, Q. Xu, Adsorption of cationic dye (methylene blue) from aqueous solution using poly(cyclotriphosphazene-co-4,4′-sulfonyldiphenol) nanospheres, Appl. Surf. Sci. 289 (2014) 495–501.
[34] A. Özer, D. Özer, The adsorption of Cr(VI) on sulphuric acid-treated wheat bran, Environ. Technol. 25 (2004) 689–697.
[35] L.H. Ai, J. Jiang, Removal of methylene blue from aqueous solution with self-assembled cylindrical graphene-carbon nanotube hybrid, Chem. Eng. J. 192 (2012) 156–163.

[36] W.H. Cheung, Y.S. Szeto, G. McKay, Intraparticle diffusion processes during acid dye adsorption onto chitosan, Bioresour. Technol. 98 (2007) 2897–2904.
[37] A. Murugesan, L. Ravikumar, V. SathyaSelvaBala, P. SenthilKumar, T. Vidhyadevi, S.D. Kirupha, S.S. Kalaivani, S. Krithiga, S. Sivanesan, Removal of Pb(II), Cu(II) and Cd(II) ions from aqueous solution using polyazomethineamides: Equilibrium and kinetic approach, Desalination 271 (2011) 199–208.
[38] F. Yu, Y.Q. Wu, J. Ma, C. Zhang, Adsorption of lead on multi-walled carbon nanotubes with different outer diameters and oxygen contents: Kinetics, isotherms and thermodynamics, J. Environ. Sci-China 25 (2013) 195–203.
[39] M.A. Wahab, S. Jellali, N. Jedidi, Ammonium biosorption onto sawdust: FTIR analysis, kinetics and adsorption isotherms modeling, Bioresour. Technol. 101 (2010) 5070–5075.
[40] M.S. Tanyildizi, Modeling of adsorption isotherms and kinetics of reactive dye from aqueous solution by peanut hull, Chem. Eng. J. 168 (2011) 1234–1240.
[41] J.F. Gao, Q. Zhang, K. Su, R.N. Chen, Y.Z. Peng, Biosorption of Acid Yellow 17 from aqueous solution by non-living aerobic granular sludge, J. Hazard. Mater. 174 (2010) 215–225.
[42] Y. Bayrak, Y. Yesiloglu, U. Gecgel, Adsorption behavior of Cr(VI) on activated hazelnut shell ash and activated bentonite, Microporous Mesoporous Mater. 91 (2006) 107–110.
[43] G. McKay, M.S. Otterburn and A.G. Sweeney, The removal of colour from effluent using various adsorbents—III. Silica: Rate processes, Water. Res., 14 (1980) 15–20.
[44] Y.H. Li, Q.J. Du, T.H. Liu, J.K. Sun, Y.H. Wang, S.L. Wu, Z.H. Wang, Y.Z. Xia, L.H. Xia, Methylene blue adsorption on graphene oxide/calcium alginate composites, Carbohydr. Polym. 95 (2013) 501–507.
[45] W.H. Zou, K. Li, H.J. Bai, X.L. Shi, R.P. Han, Enhanced cationic dyes removal from aqueous solution by oxalic acid modified rice husk, J. Chem. Eng. Data 56 (2011) 1882–1891.
[46] J.Y. Song, W.H. Zou, Y.Y. Bian, F.Y. Su, R.P. Han, Adsorption characteristics of methylene blue by peanut husk in batch and column modes, Desalination 265 (2011) 119–125.
[47] Y.S. Aldegs, M.I. Elbarghouthı, A.H. Elsheıkh, G.A. Walker, Effect of solution pH, ionic strength, and temperature on adsorption behavior of reactive dyes on activated carbon, Dyes Pigm. 77 (2008) 16–23.
[48] C.Y. Kuo, C.H. Wu, J.Y. Wu, Adsorption of direct dyes from aqueous solutions by carbon nanotubes: Determination of equilibrium, kinetics and thermodynamics parameters, J. Colloid Interface Sci. 327 (2008) 308–315.
[49] N. Nasuha, B.H. Hameed, Adsorption of methylene blue from aqueous solution onto NaOH-modified rejected tea, Chem. Eng. J. 166 (2011) 783–786.